学位論文（博士）

Effect of Paxillin Expression and Phosphorylation on Colorectal Cancer Prognosis and Metastasis

(Paxillinの発現およびリン酸化が大腸癌の予後および転移に及ぼす影響)

氏名　鄭　桓宇

所属　山口大学大学院医学系研究科

医学専攻　消化器・腫瘍外科学講座

令和 6年 1月

目　次

１．要旨

Background/Aim: Colorectal cancer (CRC) is the third most common cancer worldwide, and metastasis is strongly associated with poor prognosis in patients with CRC. We have previously found that the expression and phosphorylation of paxillin (PXN) play an important role in the metastatic potential of breast cancer. This study examined the potential role of PXN in CRC metastasis. *Materials and Methods:* Resected tumor specimens from 92 patients with CRC were subjected to immunohistochemical analysis of PXN levels. Three human CRC cell lines, HCT116, LoVo, and SW480 were used for scratch and transwell invasion assays to examine the effects of PXN over-expression. RNA sequencing was performed to obtain the expression profiles under PXN over-expression. *Results:* High levels of PXN were significantly correlated with advanced stage, higher carcinoembryonic antigen and carbohydrate antigen 19-9 levels, and poorer overall survival. The migration ability of CRC cells was enhanced by exogenous PXN over-expression, but this enhancement was not observed in cells harboring exogenously mutated PXN at Tyr31 or Tyr88 phosphorylation sites. In PXN-over-expressing cells, TNF-α signaling *via* NFκB was positively enriched. *Conclusion:* PXN expression and phosphorylation at Tyr31 or Tyr88 may influence the migration and invasion of CRC cells. PXN expression and phosphorylation at Tyr31 or Tyr88 are promising targets for evaluating prognosis and treating CRC.

2．背景

Colorectal cancer (CRC) represents a significant global healthcare challenge, ranking as the third most commonly diagnosed cancer and the third most common cause of cancer-related deaths in both men and women in the United States (1). Globally, over one million new cases of CRC are diagnosed, and CRC accounts for 10% of all newly diagnosed cancers and cancer-related fatalities annually (2, 3). Despite advancements in screening methods and clinical therapy regimens, most newly diagnosed patients have already developed metastases (4, 5). Liver metastasis is notably frequent in CRC, occurring in 50–60% of cases. Owing to the lack of effective therapies, the overall 5-year survival rate of patients with metastatic CRC remains poor (6). Distant metastasis is the leading cause of death in patients with CRC. However, the mechanism underlying CRC metastasis remains unclear.

The key steps in cancer metastasis are tumor cell migration and invasion, both of which require cytoskeletal rearrangement (7-9). Actin stress fibers are higher-order cytoskeletal structures composed of interlinked actin filament bundles that play pivotal roles in cell migration and invasion (10-12). The key regulators of actin cytoskeleton dynamics are the actin stress fibers connected to focal adhesions and focal adhesion-associated proteins, including paxillin (PXN) and focal adhesion kinase (13). Fyn tyrosine kinase is involved in actin stress fiber formation through the activation of Rho-kinase (14). Recently, we identified PXN as a novel signaling molecule that mediates

actin stress fiber formation and cell migration by directly binding to active Fyn (15).

PXN, a critical focal adhesion protein, has multiple cellular functions, such as migration and invasion (16, 17), apoptosis (18, 19), and autophagy (20, 21). PXN is regulated by tyrosine and serine phosphorylation (22, 23). Recent studies demonstrated the essential role of PXN in promoting cell invasion during breast cancer metastasis (24, 25). In addition, we reported that high PXN expression is associated with poor prognosis of breast cancer, and that phosphorylation of Tyr31 in PXN affects the migration of breast cancer cells (25). It has also been reported that PXN expression in CRC is significantly higher in tumor tissues, and that elevated PXN expression is associated with poor prognosis in patients with CRC (26-29). However, the underlying molecular mechanisms by which PXN expression and phosphorylation promote CRC metastasis have not been completely elucidated.

３．目的

This study investigated the role of PXN in the migration and invasion of CRC cells.

４．方法

Patients. Resected tumor specimens from 92 patients with CRC were used in this study. All patients underwent cancer therapy at Yamaguchi University Hospital (Ube, Japan) between January 2008 and December 2019. The study protocol was approved

by the Institutional Review Board of Yamaguchi University Hospital (H2022-177) and conducted in accordance with the Declaration of Helsinki. All the patients provided written informed consent to participate in the study.

Cell lines. The human CRC cell lines HCT116 (CCL-247) and SW480 (CCL-228) were purchased from American Type Culture Collection (Manassas, VA, USA) and LoVo (JCRB9083) was purchased from the Japanese Collection of Research Bioresources Cell Bank (Osaka, Japan). Cells were cultured in Dulbecco's modified Eagle Medium (DMEM; Nissui Pharmaceutical, Tokyo, Japan) containing 10% heat-inactivated fetal bovine serum (FBS; Thermo Fisher Scientific, Kanagawa, Japan), penicillin (100 U/ml), streptomycin (100 µg/ml), and sodium bicarbonate (1.5 g/l) at 37°C in a humidified atmosphere with 5% CO_2.

Plasmid constructs and transfection. The HaloTag full-length PXN (FHC10852, 1-1,671 bp) plasmid was purchased from Promega (Tokyo, Japan). Non-phosphorylated mutants of HaloTag PXN, Y31F, Y88F, and Y31/88F, were obtained by mutating the corresponding tyrosines to phenylalanine. For plasmid transfection, Lipofectamine™ 3000 Reagent (Thermo Fisher Scientific) was used according to the manufacturer's protocol. Briefly, 3×10^5 cells were seeded into 6-well plates containing medium without penicillin and streptomycin. After 24 h, cells were transfected with Lipofectamine™

3000 Reagent (6 μl) and one of the plasmids (2 μg), and the medium was replaced after 6 h of transfection. Cell transfection efficiency was analyzed using the HaloTag TMR Direct Ligand (Promega) after 24 h of transfection.

Immunohistochemistry. PXN expression in CRC tissues was detected by immunohistochemical (IHC) staining. The staining was performed on 4 μm formalin-fixed paraffin-embedded slides. The samples were deparaffinized in xylene and hydrated in graded alcohols and antigen retrieval was performed in EDTA buffer (pH 9.0) and heating in a microwave at 95°C for 40 min. After endogenous peroxidase and nonspecific protein blocking, the slides were incubated with monoclonal anti-PXN antibody (1:600; ab32115, Abcam, Tokyo, Japan) and incubated at 4°C overnight. The next day, after washing 3 times with PBS, the slides were incubated with the corresponding secondary antibody (K5007; Dako, Tokyo, Japan) for 30 min. Finally, the samples were visualized with 3,3'-diaminobenzidine chromogen and counterstained with Mayer's hematoxylin.

The histochemical scoring method described below was used to assess PXN expression levels in the specimens. Briefly, the method focused on both the staining intensity and the proportion of stained cells at each intensity level. The intensity values were as follows: 0 (no staining), 1 (weak staining), 2 (moderate staining), and 3 (strong staining) (Figure 1). The proportion scores were as follows: 0 (< 10%), 1 (11–25%), 2

(51–75%), and 3 (> 76%). The final PXN score was calculated as intensity × proportion (range=0–12). Immunohistochemical staining was visualized using an all-in-one fluorescence microscope BZ-X710 (KEYENCE, Osaka, Japan) and confirmed by a professional pathologist (D.C.).

Scratch assay. The scratch assay was performed as described previously (25). When the cell confluence reached 90–100% in 6-well plates, cells were starved in FBS-free medium for 24 h. The cells were then scratched using a 200 μl micropipette tip. Cell migration was observed using an all-in-one fluorescence microscope BZ-X710 (KEYENCE). The data were used for quantitative analyses of cell migration using NIH Image J software (U. S. National Institutes of Health, Bethesda, Maryland, USA). The migration rate was calculated as follows: % closure = (scratch width at 0 h − scratch width at 24 h)/scratch width at 0 h × 100.

Transwell Invasion assay. Cell invasion was determined using a Corning invasion chamber 24-well plate (354480; Corning Japan, Shizuoka, Japan), as described previously (25). Cells (3×10^5) suspended in serum-free medium were placed in the upper chamber coated with Matrigel. Medium supplemented with 10% FBS was added to the lower compartment. After culturing for 24 h, invading cells on the underside of the membrane were fixed with formaldehyde (4%) for 15 min and stained with crystal

violet (0.1%) for 30 min. The cells were visualized under a bright-field microscope at 20 × magnification (KEYENCE) and counted in three random areas.

RNA sequencing. Total RNA was isolated using the miRNeasy Mini Kit (Qiagen, Tokyo, Japan). Sequencing libraries were constructed using TruSeq Stranded Total RNA with a Ribo-Zero Gold LT Sample Prep kit (Illumina, Tokyo, Japan) according to the manufacturer's instructions. The paired-end fragments were sequenced using the NextSeq 500 sequencing platform (Illumina). After quality control, filtered short reads were mapped to the reference genome (hg38) using STAR (version 2.5.1b) (30). Strand-specific fragment counts were obtained using RSEM (version 1.3.3) (31) and normalized with the trimmed mean of M-values method (32) using the TCC package (33, 34). The edgeR package (version 3.28.1) (35, 36) was used to identify the differentially expressed genes (DEGs). Gene set enrichment analysis (GSEA) was performed using the Java command line program, GSEA2 (version 2.2.1), and Molecular Signatures Database v7.4 (37).

Statistical analysis. Each experiment was repeated at least thrice. Data are expressed as means ± standard deviation. Differences between groups were estimated using one-way analysis of variance, Tukey–Kramer multiple comparison, Mann–Whitney *U* test, or paired *t*-test. Categorical variables were compared using Fisher's exact test. Survival

curves for overall survival (OS) were calculated using the Kaplan–Meier method and analyzed using the log-rank test. Statistical analyses were performed using the R software (version 3.6.1; R Foundation for Statistical Computing, Vienna, Austria). Statistical significance was set at $p<0.05$.

４．結果

Association of tissue PXN expression with prognosis of CRC. The cut-off value (high: intensity × area ≥ 6) that divided the PXN level into high and low was determined using the time-dependent receiver operating characteristic (ROC) curve and the closest-to-the-top-left index. Patients with CRC having high PXN expression had significantly poorer outcomes in terms of OS than those with low PXN expression ($p<0.001$, Figure 2). The survival rates of patients with high PXN levels at 3, 5, and 10 years were 46.0%, 22.0%, and 8.0%, respectively. The survival rates of patients with low PXN at 3, 5, and 10 years were 92.9%, 78.6%, and 23.8%, respectively.

Among the clinicopathological features, concentrations of carcinoembryonic antigen (CEA) and carbohydrate antigen 19-9 (CA 19-9) were significantly higher in the PXN-high group than in the PXN-low group, although there were no significant differences in age or sex between these groups (Table I). PXN levels increased with stage progression, reaching the highest level at stage 4 (Figure 3A). Moreover, PXN expression was significantly higher in liver metastases than in primary CRC tissues in identical stage 4 cases (Figure 3B).

Cell migration ability and PXN expression in cell lines. The expression levels of *PXN* at the RNA level in the three human CRC cell lines, HCT116, LoVo, and SW480, were examined using RNA sequencing (Figure 4). Cells transfected with *PXN* expressing vectors showed higher PXN transcripts per million than cells transfected with an empty vector. More than 90% of the reads from cells harboring *PXN* expression vectors with mutations were confirmed to have corresponding mutations.

Both scratch and transwell invasion assays showed that the motility of HCT116, LoVo, and SW480 cells over-expressing wild-type *PXN* was increased compared to that of cells transfected with empty vector or vectors with mutations at tyrosine 31 or 88 of *PXN* (Figure 5).

Expression profile of PXN over-expressing cells. In the three cell lines, gene set enrichment analysis using the read counts from RNA sequencing revealed that, compared to cells harboring empty vector or *PXN* with mutation vector, wild-type *PXN*-over-expressing cells had a significantly enriched signature of tumor necrosis factor (TNF)-α signaling *via* NFκB (Figure 6).

5．考察

PXN expression is associated with poor prognosis of breast cancer, and phosphorylation of Tyr31 in PXN affects the migration of breast cancer cells (25).

Similarly, PXN expression is significantly higher in CRC tissues, and elevated PXN expression is associated with poor prognosis in patients with CRC (26-29). However, the molecular mechanisms through which PXN expression and phosphorylation promote CRC metastasis remain unclear. Here, we investigated these mechanisms. Our findings indicate that high PXN expression is associated with poor prognosis in patients with CRC, and that the phosphorylation of Tyr31 and Tyr88 in PXN is a key factor in determining CRC cell migration.

PXN is highly expressed in many malignant tumors, affecting recurrence and metastasis in cancers such as gastric (38), breast (17), and esophageal (39) cancer. Consistently, patients with high PXN expression showed significantly shorter OS than those with low PXN expression (Figure 2). Moreover, PXN expression levels increased with tumor stage (Figure 3A) and the PXN level was significantly higher in liver metastases than in the corresponding primary CRC tissues (Figure 3B). PXN expression was also significantly correlated with CEA and CA19-9 levels (Table I). In addition, our *in vitro* analyses showed that PXN over-expression promoted the migration and invasion abilities of CRC cells, which were diminished by mutations in Tyr31 or 88 of PXN (Figure 5). Consistent with our results, mutations in Tyr31 of PXN have a crucial effect on the migration of breast cancer cells (25).

Previous reports have indicated that PXN functions through several pathways, such as the integrin signaling (40), the mitogen-activated protein kinase signaling (41),

and the Rho GTPase signaling (15) pathways. Our comprehensive expression data from RNA sequencing followed by GSEA showed that there is positive enrichment of TNF-α signaling in the PXN-over-expressing cells (Figure 6). TNF has long been considered a therapeutic target to inhibit tumors, but recent studies have contradicted this notion, suggesting that TNF-α is one of the factors contributing to the deterioration of certain tumors (42, 43). Weitzenfeld *et al*. found that TNF promotes the progression and metastasis of breast cancer through various pathways (44). In neutrophils, it was reported that TNF-α stimulates the tyrosine phosphorylation of PXN (45). In addition, Zhang *et al*. indicated that repression of PXN *via* a microRNA, miR-24, suppresses TNF-α production and cytotoxicity of natural killer cells from patients with CRC (46). In conjunction with our research, the results indicate that up-regulation of TNF-α signaling by PXN phosphorylation may contribute to tumor progression and metastasis.

This study has some limitations: Analysis of PXN phosphorylation in clinical samples, experiments using animal models, examination of the effects of other phosphorylation sites of PXN, and the detailed molecular mechanisms upstream and downstream of PXN on poor prognostic features of CRC were not examined. Nevertheless, our study indicates that PXN may play a crucial role in the migration of CRC cells *via* its expression and phosphorylation at Tyr31 and Tyr88.

6．結語

Our findings indicated that the expression and phosphorylation of PXN at Tyr31 or Tyr88 may influence the migration and invasion of CRC cells. Therefore, phosphorylation of Tyr31 or Tyr88 in PXN is an important and meaningful target for the prognosis and treatment of CRC.

７．謝辞

本研究にあたり、ご指導いただきました永野浩昭先生に深甚なる謝意を表します。また、山口大学消化器・腫瘍外科学の皆様に深謝いたします。

８．参考文献

1 Siegel RL, Wagle NS, Cercek A, Smith RA, Jemal A: Colorectal cancer statistics, 2023. CA Cancer J Clin 73(3): 233-254, 2023. DOI: 10.3322/caac.21772

2 Ismaili N: Treatment of colorectal liver metastases. World J Surg Oncol 9: 154, 2011. DOI: 10.1186/1477-7819-9-154

3 Arnold M, Sierra MS, Laversanne M, Soerjomataram I, Jemal A, Bray F: Global patterns and trends in colorectal cancer incidence and mortality. Gut 66(4): 683-691, 2017. DOI: 10.1136/gutjnl-2015-310912

4 Ueno H, Nagtegaal ID, Quirke P, Sugihara K and Ajioka Y: Tumor deposits in colorectal cancer: Refining their definition in the tnm system. Ann Gastroenterol Surg 7(2): 225-235, 2023. DOI: 10.1002/ags3.12652

5 Margonis GA and Vauthey JN: Precision surgery for colorectal liver metastases: Current knowledge and future perspectives. Ann Gastroenterol Surg 6(5): 606-615, 2022. DOI: 10.1002/ags3.12591

6 Xie YH, Chen YX and Fang JY: Comprehensive review of targeted therapy for colorectal cancer. Signal Transduct Target Ther 5(1): 22, 2020. DOI: 10.1038/s41392-019-0102-5

7 Yamaguchi H and Condeelis J: Regulation of the actin cytoskeleton in cancer cell migration and invasion. Biochim Biophys Acta 1773(5): 642-652, 2007. DOI: 10.1016/j.bbamcr.2006.07.001

8 Aseervatham J: Cytoskeletal remodeling in cancer. Biology (Basel) 9(11), 2020. DOI: 10.3390/biology9110385

9 Wilson AL, Schrecengost RS, Guerrero MS, Thomas KS and Bouton AH: Breast cancer antiestrogen resistance 3 (BCAR3) promotes cell motility by regulating actin cytoskeletal and adhesion remodeling in invasive breast cancer cells. PLoS One 8(6): e65678, 2013. DOI: 10.1371/journal.pone.0065678

10 Fischer RS, Sun X, Baird MA, Hourwitz MJ, Seo BR, Pasapera AM, Mehta SB, Losert W, Fischbach C, Fourkas JT and Waterman CM: Contractility, focal adhesion orientation, and stress fiber orientation drive cancer cell polarity and migration along wavy ECM substrates. Proc Natl Acad Sci U S A 118(22), 2021. DOI: 10.1073/pnas.2021135118

11 Balta E, Kramer J and Samstag Y: Redox regulation of the actin cytoskeleton in cell migration and adhesion: On the way to a spatiotemporal view. Front Cell Dev Biol 8: 618261, 2020. DOI: 10.3389/fcell.2020.618261

12 Olson MF and Sahai E: The actin cytoskeleton in cancer cell motility. Clin Exp Metastasis 26(4): 273-287, 2009. DOI: 10.1007/s10585-008-9174-2

13 Hu YL, Lu S, Szeto KW, Sun J, Wang Y, Lasheras JC and Chien S: Fak and paxillin dynamics at focal adhesions in the protrusions of migrating cells. Sci Rep 4: 6024, 2014. DOI: 10.1038/srep06024

14 Xu D, Kishi H, Kawamichi H, Kajiya K, Takada Y and Kobayashi S: Involvement of fyn tyrosine kinase in actin stress fiber formation in fibroblasts. FEBS Lett 581(27): 5227-5233, 2007. DOI: 10.1016/j.febslet.2007.10.010

15 Zhang Y, Kishi H, Morita T and Kobayashi S: Paxillin controls actin stress fiber formation and migration of vascular smooth muscle cells by directly binding to the active fyn. FASEB J 35(12): e22012, 2021. DOI: 10.1096/fj.202101035RR

16 López-Colomé AM, Lee-Rivera I, Benavides-Hidalgo R and López E: Paxillin: A crossroad in pathological cell migration. J Hematol Oncol 10(1): 50, 2017. DOI: 10.1186/s13045-017-0418-y

17 Deakin NO and Turner CE: Distinct roles for paxillin and hic-5 in regulating breast cancer cell morphology, invasion, and metastasis. Mol Biol Cell 22(3): 327-341, 2011. DOI: 10.1091/mbc.E10-09-0790

18 Nah AS and Chay KO: Roles of paxillin phosphorylation in il-3 withdrawal-induced ba/f3 cell apoptosis. Genes Genomics 41(2): 241-248, 2019. DOI: 10.1007/s13258-018-00779-2

19 Chay KO, Park SS and Mushinski JF: Linkage of caspase-mediated degradation of paxillin to apoptosis in BA/F3 murine pro-b lymphocytes. J Biol Chem 277(17): 14521-14529, 2002. DOI: 10.1074/jbc.M111639200

20 Sharifi MN, Mowers EE, Drake LE, Collier C, Chen H, Zamora M, Mui S and Macleod KF: Autophagy promotes focal adhesion disassembly and cell motility of

metastatic tumor cells through the direct interaction of paxillin with lc3. Cell Rep 15(8): 1660-1672, 2016. DOI: 10.1016/j.celrep.2016.04.065

21 Zhang X, Bai Y, Huang L, Liu S, Mo Y, Cheng W, Wang G, Cao Z, Chen X, Cui H, Qi L, Ma L, Liu M, Guan XY and Ma NF: Chd1l augments autophagy-mediated migration of hepatocellular carcinoma through targeting zkscan3. Cell Death Dis 12(10): 950, 2021. DOI: 10.1038/s41419-021-04254-x

22 Zaidel-Bar R, Milo R, Kam Z and Geiger B: A paxillin tyrosine phosphorylation switch regulates the assembly and form of cell-matrix adhesions. J Cell Sci 120(Pt 1): 137-148, 2007. DOI: 10.1242/jcs.03314

23 Abou Zeid N, Vallés AM and Boyer B: Serine phosphorylation regulates paxillin turnover during cell migration. Cell Commun Signal 4: 8, 2006. DOI: 10.1186/1478-811X-4-8

24 Xu W, Alpha KM, Zehrbach NM and Turner CE: Paxillin promotes breast tumor collective cell invasion through maintenance of adherens junction integrity. Mol Biol Cell 33(2): ar14, 2022. DOI: 10.1091/mbc.E21-09-0432

25 Zhang Y, Zheng H, Xu M, Maeda N, Tsunedomi R, Kishi H, Nagano H and Kobayashi S: Fyn-mediated paxillin tyrosine 31 phosphorylation regulates migration and invasion of breast cancer cells. Int J Mol Sci 24(21), 2023. DOI: 10.3390/ijms242115980

26 Qin J, Wang F, Jiang H, Xu J, Jiang Y and Wang Z: Microrna-145 suppresses cell migration and invasion by targeting paxillin in human colorectal cancer cells. Int J Clin Exp Pathol 8(2): 1328-1340, 2015. DOI: n/a

27 Zhao CJ, Du SK, Dang XB and Gong M: Expression of paxillin is correlated with clinical prognosis in colorectal cancer patients. Med Sci Monit 21: 1989-1995, 2015. DOI: 10.12659/MSM.893832

28 Wen L, Zhang X, Zhang J, Chen S, Ma Y, Hu J, Yue T, Wang J, Zhu J, Wu T and Wang X: Paxillin knockdown suppresses metastasis and epithelial - mesenchymal transition in colorectal cancer via the erk signalling pathway. Oncol Rep 44(3): 1105-1115, 2020. DOI: 10.3892/or.2020.7687

29 Wu JN, Lin L, Luo SB, Qiu XZ, Zhu LY, Chen D, Wei ED, Fu ZH, Qin MB, Liang ZH, Huang JA and Liu SQ: Sphk1-driven autophagy potentiates focal adhesion paxillin-mediated metastasis in colorectal cancer. Cancer Med 10(17): 6010-6021, 2021. DOI: 10.1002/cam4.4129

30 Wang T, Liu J, Shen L, Tonti-Filippini J, Zhu Y, Jia H, Lister R, Whitaker JW, Ecker JR, Millar AH, Ren B and Wang W: Star: An integrated solution to management and visualization of sequencing data. Bioinformatics 29(24): 3204-3210, 2013. DOI: 10.1093/bioinformatics/btt558

31 Li B and Dewey CN: Rsem: Accurate transcript quantification from rna-seq data with or without a reference genome. BMC Bioinformatics 12: 323, 2011. DOI: 10.1186/1471-2105-12-323

32 Robinson MD and Oshlack A: A scaling normalization method for differential expression analysis of rna-seq data. Genome Biol 11(3): R25, 2010. DOI: 10.1186/gb-2010-11-3-r25

33 Sun J, Nishiyama T, Shimizu K and Kadota K: TCC: An R package for comparing tag count data with robust normalization strategies. BMC Bioinformatics 14: 219, 2013. DOI: 10.1186/1471-2105-14-219

34 Tang M, Sun J, Shimizu K and Kadota K: Evaluation of methods for differential expression analysis on multi-group RNA-seq count data. BMC Bioinformatics 16: 361, 2015. DOI: 10.1186/s12859-015-0794-7

35 Robinson MD, McCarthy DJ and Smyth GK: Edger: A bioconductor package for differential expression analysis of digital gene expression data. Bioinformatics 26(1): 139-140, 2010. DOI: 10.1093/bioinformatics/btp616

36 McCarthy DJ, Chen Y and Smyth GK: Differential expression analysis of multifactor RNA-seq experiments with respect to biological variation. Nucleic Acids Res 40(10): 4288-4297, 2012. DOI: 10.1093/nar/gks042

37 Subramanian A, Tamayo P, Mootha VK, Mukherjee S, Ebert BL, Gillette MA, Paulovich A, Pomeroy SL, Golub TR, Lander ES and Mesirov JP: Gene set

enrichment analysis: A knowledge-based approach for interpreting genome-wide expression profiles. Proc Natl Acad Sci U S A 102(43): 15545-15550, 2005. DOI: 10.1073/pnas.0506580102

38 Chen DL, Wang ZQ, Ren C, Zeng ZL, Wang DS, Luo HY, Wang F, Qiu MZ, Bai L, Zhang DS, Wang FH, Li YH and Xu RH: Abnormal expression of paxillin correlates with tumor progression and poor survival in patients with gastric cancer. J Transl Med 11: 277, 2013. DOI: 10.1186/1479-5876-11-277

39 Cai HX, Yang LC, Song XH, Liu ZR, Chen YB and Dong GK: Expression of paxillin and FAK mRNA and the related clinical significance in esophageal carcinoma. Mol Med Rep 5(2): 469-472, 2012. DOI: 10.3892/mmr.2011.664

40 Ripamonti M, Wehrle-Haller B and de Curtis I: Paxillin: A hub for mechano-transduction from the β3 integrin-talin-kindlin axis. Front Cell Dev Biol 10: 852016, 2022. DOI: 10.3389/fcell.2022.852016

41 Sen A, O'Malley K, Wang Z, Raj GV, Defranco DB and Hammes SR: Paxillin regulates androgen- and epidermal growth factor-induced mapk signaling and cell proliferation in prostate cancer cells. J Biol Chem 285(37): 28787-28795, 2010. DOI: 10.1074/jbc.M110.134064

42 Balkwill F: Tumour necrosis factor and cancer. Nat Rev Cancer 9(5): 361-371, 2009. DOI: 10.1038/nrc2628

43 Bertazza L and Mocellin S: The dual role of tumor necrosis factor (TNF) in cancer biology. Curr Med Chem 17(29): 3337-3352, 2010. DOI: 10.2174/092986710793176339

44 Weitzenfeld P, Meron N, Leibovich-Rivkin T, Meshel T and Ben-Baruch A: Progression of luminal breast tumors is promoted by ménage à trois between the inflammatory cytokine tnfα and the hormonal and growth-supporting arms of the tumor microenvironment. Mediators Inflamm 2013: 720536, 2013. DOI: 10.1155/2013/720536

45 Fuortes M, Jin WW and Nathan C: Beta 2 integrin-dependent tyrosine phosphorylation of paxillin in human neutrophils treated with tumor necrosis factor. J Cell Biol 127(5): 1477-1483, 1994. DOI: 10.1083/jcb.127.5.1477

46 Zhang LL, Zhang LF and Shi YB: Mir-24 inhibited the killing effect of natural killer cells to colorectal cancer cells by downregulating paxillin. Biomed Pharmacother 101: 257-263, 2018. DOI: 10.1016/j.biopha.2018.02.024

９．図表

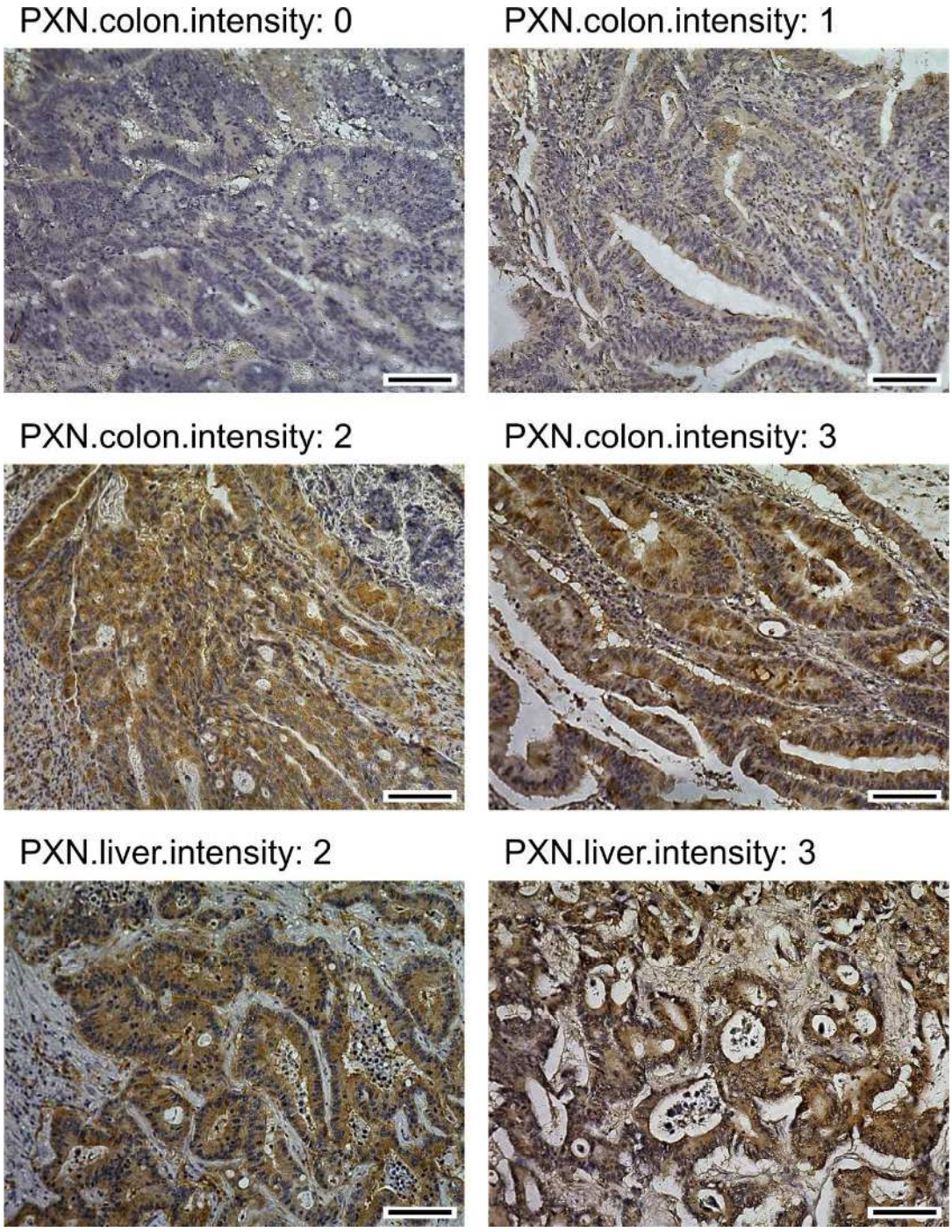

Figure 1. Immunohistochemistry for paxillin (PXN) using primary colorectal and liver metastatic tissues. Representative images of PXN staining with the following intensities: negative (0), weak (1), moderate (2), and strong (3). PXN staining of vessels was simultaneously evaluated as a positive control. The scale bar represents 100 μm.

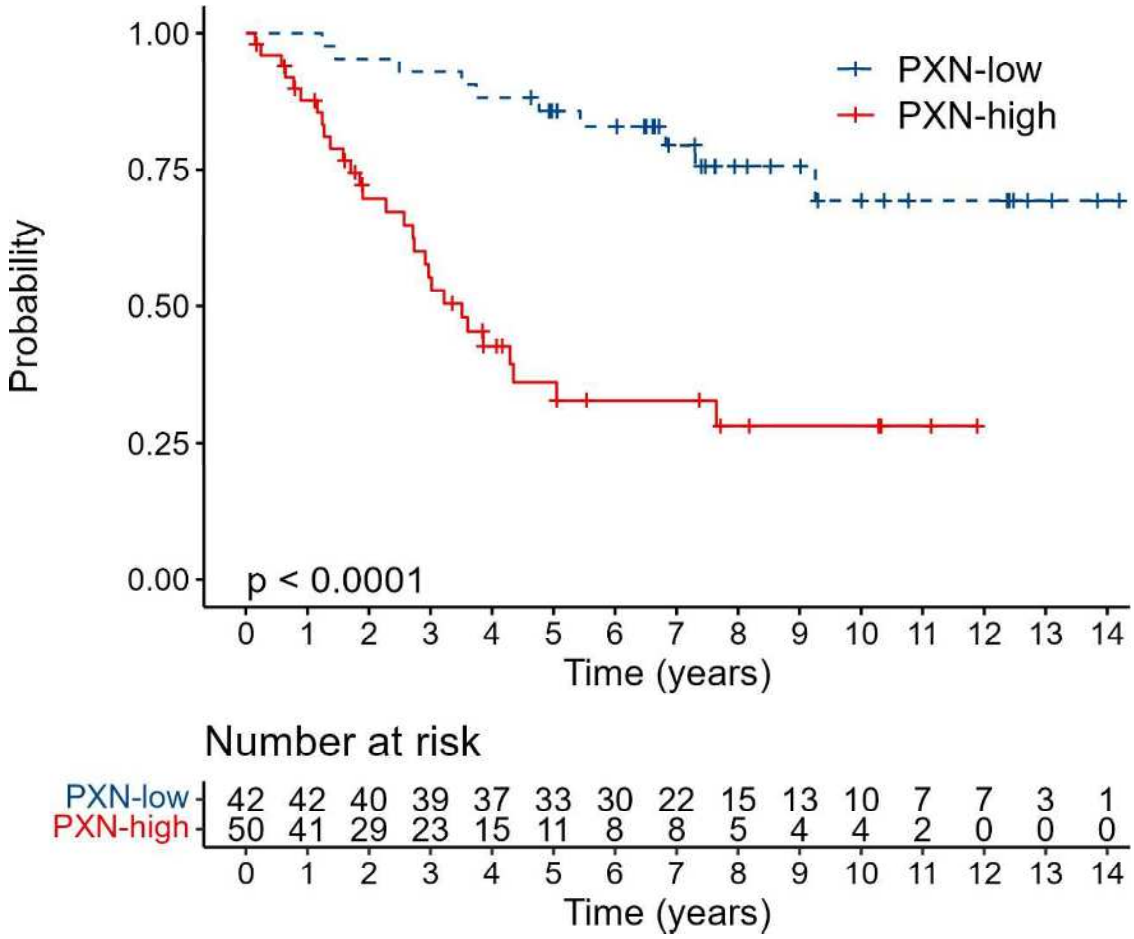

Figure 2. Kaplan–Meier curves for the overall survival (OS) of patients according to PXN levels in colorectal cancer (CRC) tissues. Patients with CRC were divided into two groups, low and high, based on the PXN levels in tumor cells. The cut-off PXN expression, ≥ 6 (intensity × area), was determined using the time-dependent ROC curve analysis.

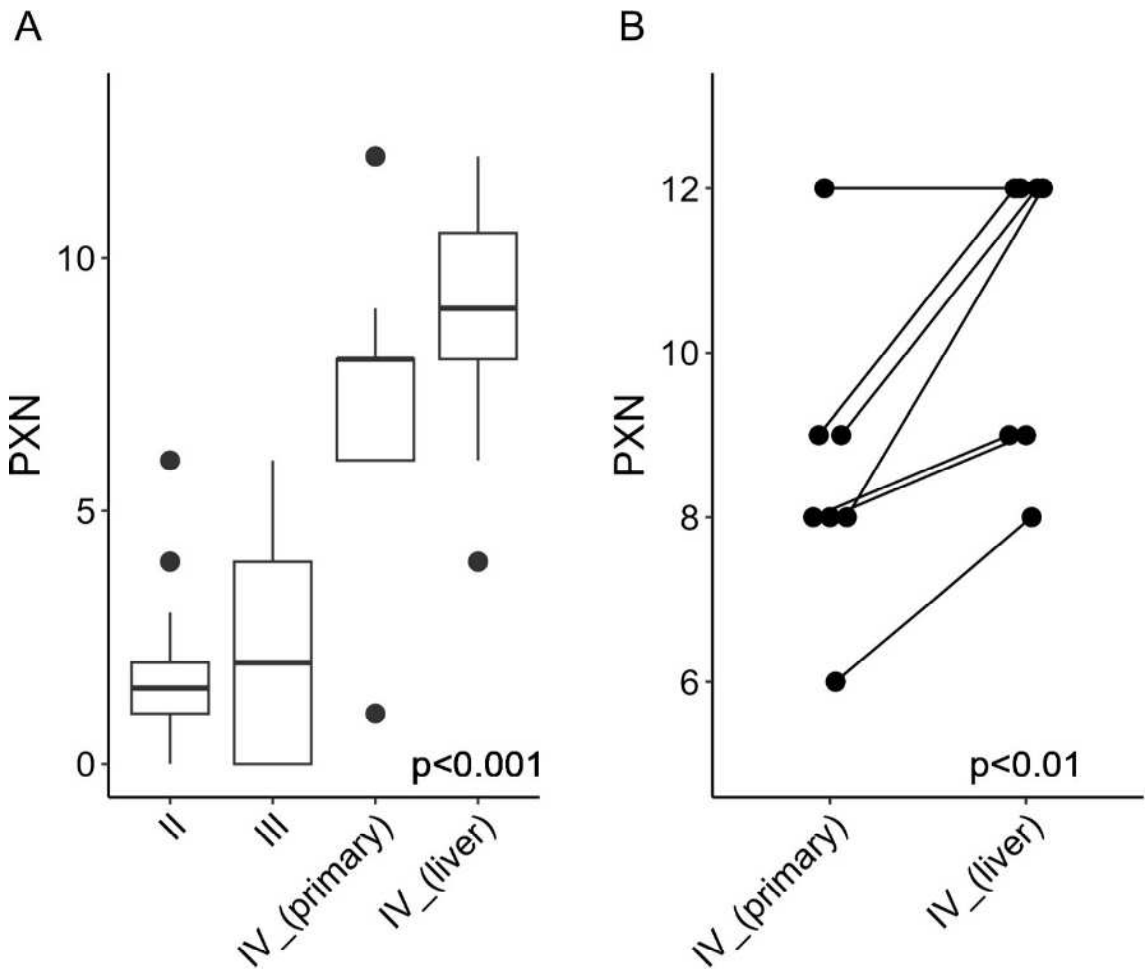

Figure 3. Expression of PXN in CRC tissues. PXN levels at each pathological stage (stages II–IV) were measured using immunohistochemistry. *p* Values were calculated using one-way analysis of variance (A) and paired *t*-test (B).

A

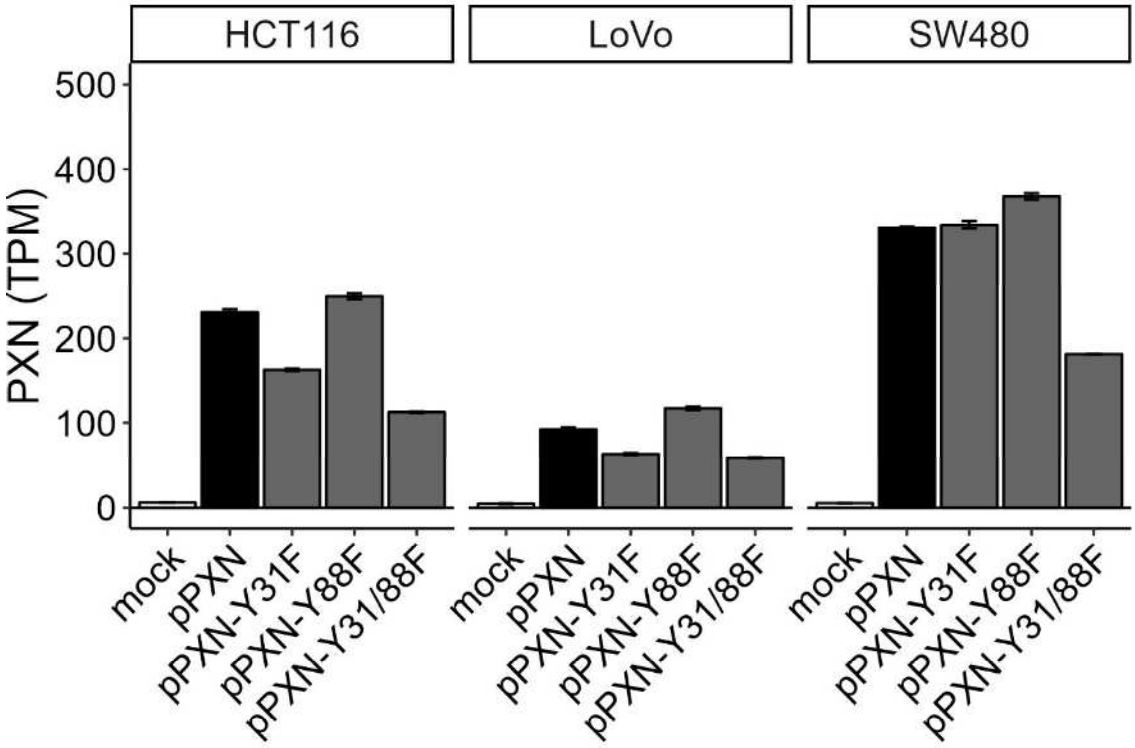

B

	% of reads with mutation					
	HCT116		LoVo		SW480	
	Y31F	Y88F	Y31F	Y88F	Y31F	Y88F
mock	2.8	0.0	11.1	0.0	6.7	0.0
pPXN	0.5	0.1	0.9	0.3	0.7	0.2
pPXN-Y31F	97.7	0.1	95.9	0.1	96.7	0.2
pPXN-Y88F	3.0	96.4	1.2	96.8	0.9	99.2
pPXN-Y31/88F	92.9	94.3	95.0	95.8	96.0	97.6

Figure 4. Expression of PXN in PXN-transfectants. The PXN levels in the cells were determined using RNA sequencing. (A) Expression levels are presented as transcripts per million (TPM). (B) Percentage of counts with mutations in RNA sequencing. Most PXN TPMs were derived from each plasmid vector.

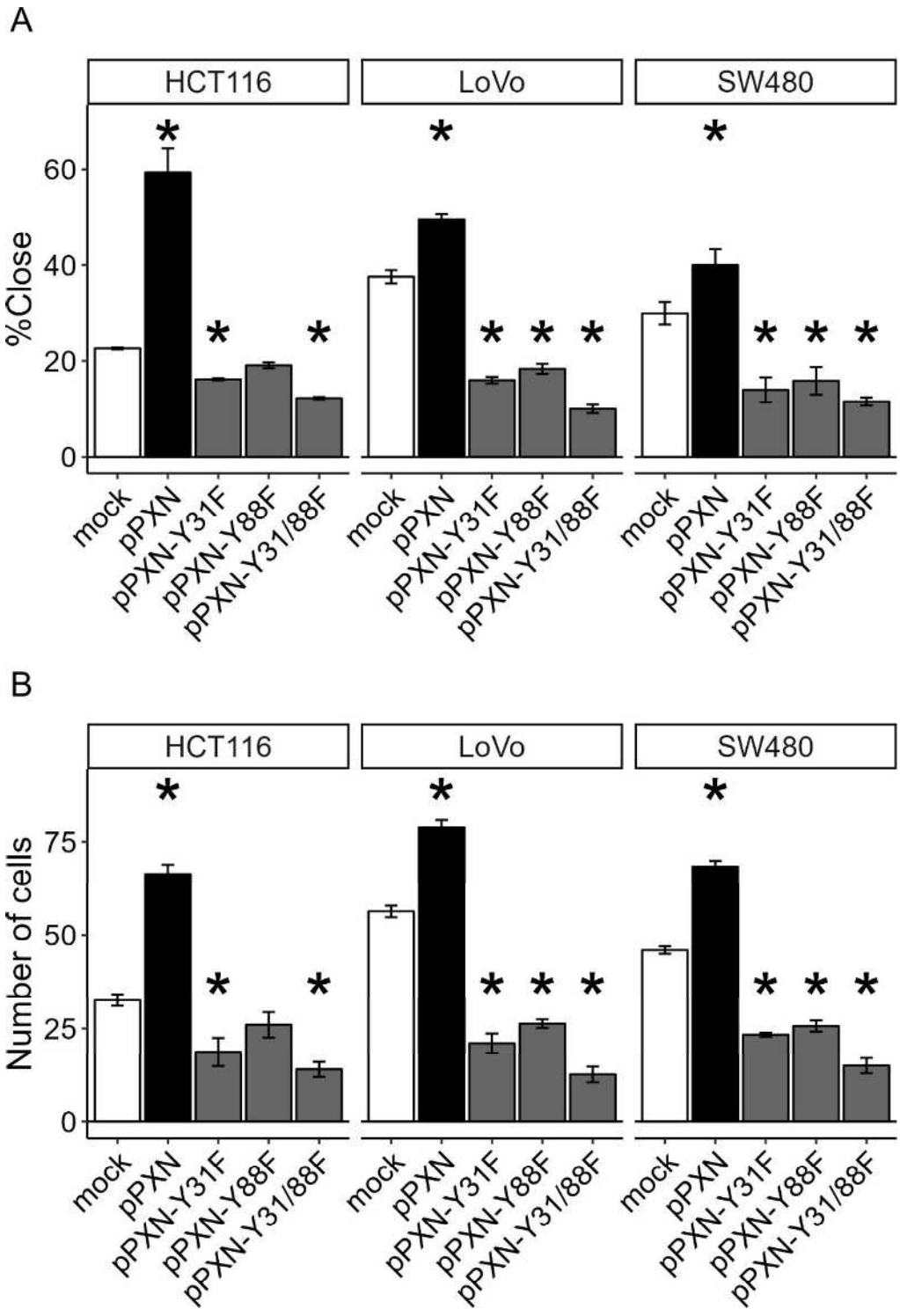

Figure 5. Cell migration abilities of PXN transfectants. The migration ability of cells transfected with each PXN encoding vector was evaluated using the scratch (A) and transwell (B) assay as described in the Materials and Methods. *p<0.05, Tukey–Kramer multiple comparison test (*vs.* mock).

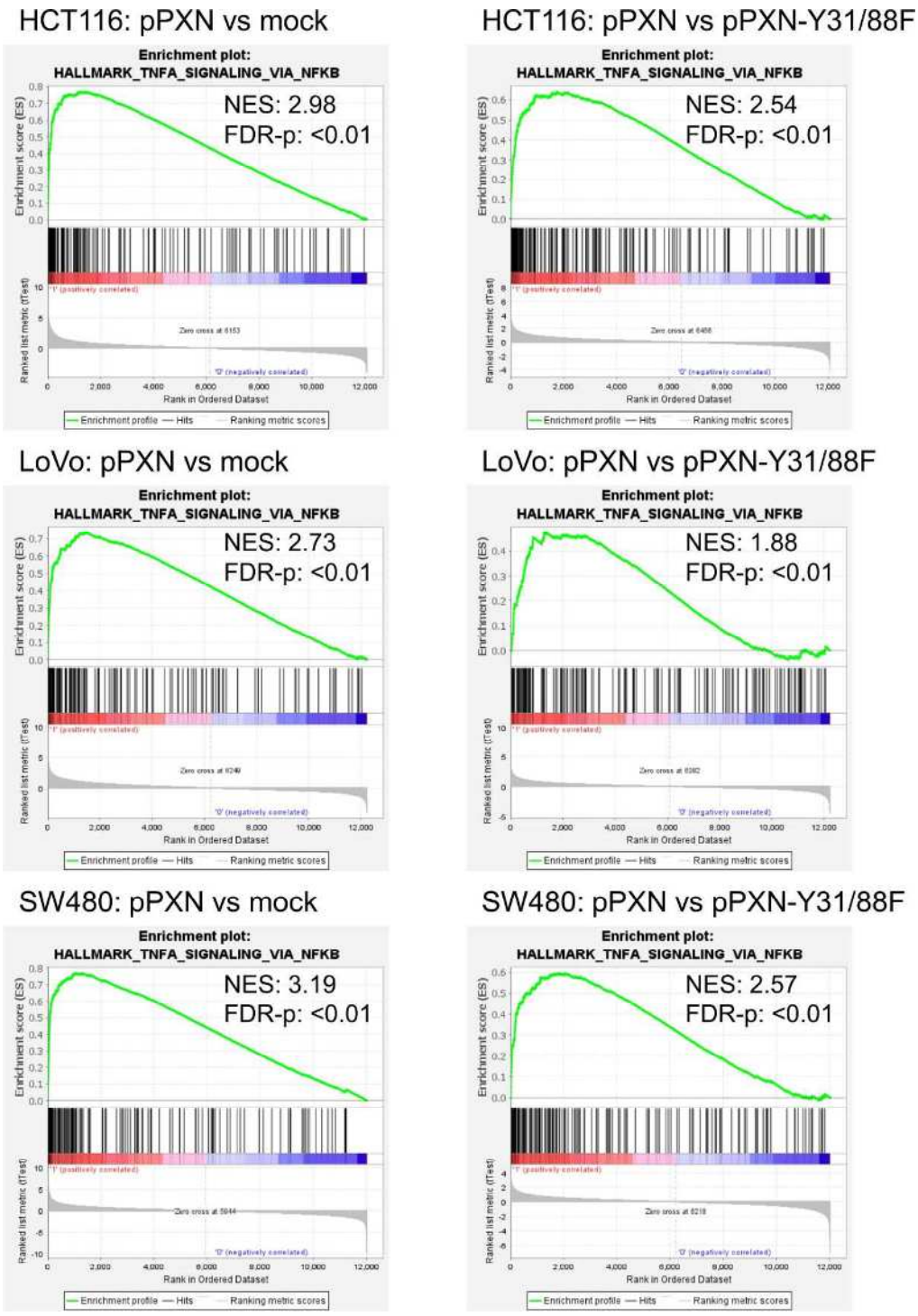

Figure 6. Enriched molecular signatures in PXN-over-expressing cells. RNA-sequence data were subjected to Gene Set Enrichment Analysis (GSEA). Cells transfected with pPXN were used as the test, and cells transfected with mock or pPXN-Y31/88F were used as the control. Enrichment plots from GSEA data show significant enrichment of TNF-α signaling *via* NF-κB. NES: Normalized enrichment score. FDR-q: *p* values adjusted using the Benjamini–Hochberg method.

Table I. Relation between PXN level and clinicopathological characteristics.

	PXN*		
	Low (n = 42)	High (n = 50)	p-Value
Age, years			
Median	69	69	0.426
(range)	(61.5–78)	(60.25–76.75)	
Sex			
Male	20	24	1.00
Female	22	26	
CEA (ng/ml)			
Median	6.15	19.9	< 0.01
(IQR)	(3.43–7.50)	(9.30–93.4)	
CA19-9 (U/ml)			
Median	12.0	57.2	< 0.01
(IQR)	(4.68–24.0)	(10.1–122.7)	
Tumor size			
Median	4	5	0.0616
(IQR)	(3.5–5.5)	(2.4–6.5)	
pStage			
II/III	41	4	< 0.01
IV	1	46	

*The cut-off value of ≥ 6 (intensity × area) for PXN-high was determined using the time-dependent ROC curve analysis. p Values were determined using the Mann–Whitney U test or Fisher's exact test.

PXN: Paxillin; CEA: carcinoembryonic antigen; CA: carbohydrate antigen; IQR: interquartile range.